Journal of Catalysis **212,** 157–172 (2002)
doi:10.1006/jcat.2002.3775

Fe–ZSM-5 Catalysts for the Selective Reduction of NO by Isobutane—The Problem of the Active Sites

Frank Heinrich,* Carmen Schmidt,* Elke Löffler,* Michael Menzel,† and Wolfgang Grünert*,[1]

*Lehrstuhl für Technische Chemie, Ruhr-Universität Bochum, D-44780 Bochum, Germany; and †Federal Institute for Materials Research and Testing (BAM), D-12489 Berlin, Germany

Received April 9, 2002; revised June 13, 2002; accepted July 31, 2002

Relations between the structure of Fe–ZSM-5 catalysts prepared by interaction of $FeCl_3$ with H–ZSM-5 and their catalytic behavior in the SCR of NO by isobutane were investigated by combining results of catalytic studies (1000 ppm NO, 1000 ppm isobutane, and 2% O_2 in He, 30,000 h^{-1}) and of physicochemical characterization (XRD, EXAFS, Mössbauer spectroscopy, TPR, IR, XPS). By variation of the preparation conditions (method of $FeCl_3$ introduction—chemical vapor deposition or solid-state ion exchange, washing intensity, calcination regime) and of the matrix (H–ZSM-5 with normal and high defect density), Fe–ZSM-5 materials with strongly varying properties (aggregation degree of the Fe phase, acidity) were obtained. Significant discrepancies between conclusions derived from EXAFS, TPR, and Mössbauer spectroscopy were ascribed to a preference of Mössbauer spectroscopy for the detection of aggregated phases and a high defectivity of Fe oxide clusters formed upon calcination. The critical step for the preparation of a highly disperse Fe phase is extensive washing after Fe introduction. The catalytic behavior of overexchanged Fe–ZSM-5 materials prepared by interaction of $FeCl_3$ with H–ZSM-5 of normal defect density was not influenced by aggregation of a significant part of the Fe phase. The comparison of their catalytic properties with those of a Fe_2O_3/H–ZSM-5 mechanical mixture and of catalysts prepared by aqueous ion exchange or by CVD of $FeCl_3$ into H–ZSM-5 of high defect density implies that the particular activity of overexchanged Fe–ZSM-5 arises from minority sites. In these, the Fe ions are probably isolated. Other Fe sites of low nuclearity appear to add to the activity. The poor SCR performance (at a given ability for isobutane activation) of Fe–ZSM-5 prepared with a defective ZSM-5 matrix may indicate that the Fe sites which provide the particular activity of overexchanged Fe–ZSM-5 require the cooperation of acidic sites. © 2002 Elsevier Science (USA)

Key Words: **deNO$_x$; hydrocarbons; isobutane; Fe–ZSM-5; EXAFS; Mössbauer spectroscopy; temperature-programmed reduction.**

INTRODUCTION

The selective catalytic reduction of nitrogen oxides by hydrocarbons (HC-SCR) has been a major topic in environmental catalysis for several years because of its promise of an elegant technology for NO_x abatement with diesel and lean-burn Otto engines (1–3). There are, however, no catalysts as yet that combine sufficient activity and stability to open this approach to commercial mobile-source applications. Overexchanged Fe–ZSM-5 (Fe/Al $\approx$ 1) as described by Feng and co-workers (4, 5), which was reported to exhibit very high activity and encouraging stability, appeared to be an attractive system, but the preparation used by these authors could not be reproduced (see, for instance, (5)). Instead, it was shown that overexchanged Fe–ZSM-5 catalysts of somewhat less favorable but still promising catalytic properties can be reproducibly prepared via a route that involves chemical vapor deposition (CVD) of $FeCl_3$ into H–ZSM-5, with subsequent washing and calcination steps (6).

With this preparation, it has been found by IR spectroscopy and other techniques that the zeolite Brønsted sites are completely consumed during the CVD of $FeCl_3$, probably by exchange with $FeCl_2^+$ entities. Upon subsequent washing and calcination steps, they are partly restored (6, 7). This indicates some mobility of the iron species leading to clustered moieties. It was proposed that Fe–O–Fe dimer species are formed predominantly (6). This suggestion has been supported on the basis of EXFAS investigations (7, 8), and the Fe–O–Fe dimer species are considered to be responsible for the high SCR activity of overexchanged Fe–ZSM-5. It should be noted, however, that clusters of different kinds (Fe_4O_4 structures) were identified earlier in an EXAFS study of Fe–ZSM-5 prepared by ion exchange from methanolic solution (9).

It was indicated in (7, 10) that even the CVD technique proposed by Sachtler *et al.* may result in catalysts containing different Fe sites. In the present study, we have compared Fe–ZSM-5 materials prepared from $FeCl_3$ via different dry techniques (CVD, solid-state ion exchange (SSIE)) with ZSM-5 of different origin and using various conditions in the washing and calcination steps. The catalysts have been characterized by various techniques: XRD, XPS, X-ray absorption spectroscopy (EXAFS, XANES), IR spectroscopy, Mössbauer spectroscopy, and temperature-programmed reduction (TPR). It will be shown that the

[1] To whom correspondence should be addressed. Fax: +49 234 321 4115. E-mail: w.gruenert@techem.ruhr-uni-bochum.de.

0021-9517/02 $35.00

characterization of overexchanged Fe–ZSM-5 by EXAFS or Mössbauer spectroscopy alone may lead to erroneous conclusions. SCR activities comparable to activity data from the literature may be obtained with materials for which a strongly different extent of clustering was observed in the characterization studies. This suggests that the activity is mainly provided by a minority species. On the other hand, a catalyst with a Fe phase of analogous structural properties but low Brønsted acidity of the support fails.

EXPERIMENTAL

Materials

Na–ZSM-5 samples were kindly supplied by Chemiewerk Bad Köstritz and Tricat Bitterfeld (both Germany). One of the products, which resulted from a synthesis with a tetrapropylammonium hydroxide template, was originally produced with the intention of ascertaining the limits of recommended synthesis conditions. It had a large quantity of nonincorporated Al and, correspondingly, of internal silanol defects and was chosen because of its abundance of defects. Both Na–ZSM-5 zeolites were transferred into the H-form by ion exchange with 0.1 M HCl, which at the same time removes extraframework aluminum. After this treatment, the Si/Al atomic ratios of the parent zeolites were ≈14 (labeled A) and ≈40 (defective, labeled B). A zeolite H-beta donated by Südchemie (Germany; $n_{Si}/n_{Al} \approx 90$) was employed to prepare a reference sample for the XANES spectra.

The chemical vapor deposition of $FeCl_3$ into these zeolites was performed in a glass apparatus in two steps. First, approximately 5 g H–ZSM-5 was dried in flowing air (≈50 ml/min) according to the following temperature protocol: a 2 K/min temperature ramp to 423 K, 15 min at 423 K, a 5 K/min temperature ramp to 823 K, 60 min at 823 K. After cooling in inert gas, anhydrous $FeCl_3$ was loaded into the glass apparatus as a second, separate layer in inert atmosphere (glove box). The setup was then heated to 573 K under flowing nitrogen (5 K/min) and kept at this temperature for ≈1 h, until $FeCl_3$ was observed to be deposited on cool walls behind the heated zone. After Fe introduction, the catalyst was repeatedly washed in deionized water, typically with a total of 1 liter per 5 g catalyst. The catalysts were then dried at room temperature. Alternatively, solid-state ion exchange was used to incorporate Fe into ZSM-5. For this purpose, 7 g of H–ZSM-5 was mixed with 3.5 g of $FeCl_3 \cdot 6\,H_2O$, and the mixture was transferred into a porcelain boat, which was heated in flowing N_2 (50 ml/min) to 573 K and kept there for 1 h. In this preparation, the washing step was omitted so that the excess iron remained in the sample.

Prior to the catalytic experiments, all catalysts except that prepared via SSIE were calcined in flowing dry air at 873 K for 1 h. In this standard calcination, the temperature was raised from room temperature to 423 K at 2 K/min, and after a 15-min isothermal period the temperature ramp was continued at 5 K/min. A preparation via CVD, washing with 1 liter water per 5 g catalyst and with a 5 K/min final temperature ramp, will be referred to as the standard preparation. The samples prepared via this route will be labeled only with the zeolite label (A or B). A reference Fe-beta sample was prepared via the same route. Deviations from this standard preparation concern the mode of Fe introduction (SSIE instead of CVD, no washing), the amount of water used for washing (10 liters instead of 1 liter, with negative results from an $AgNO_3$ test with the final effluent), and the calcination regime (temperature ramps of 10 or 0.5 K/min from room temperature to 873 K). Table 1 demonstrates how these deviations are reflected in the sample codes.

Table 1 reports also the Fe amounts introduced and the resulting Fe/Al atomic ratios. The Fe content was deduced from the XAFS spectra by comparing the edge heights obtained from these samples in repetitive runs (after washing, calcination, and catalysis, under the assumption that no Fe was lost in these steps) with the specific absorption

TABLE 1

Description of Fe–ZSM-5 Catalysts Investigated

Code	Preparation			%Fe	n_{Fe}/n_{Al}	n_{Fe}/n_{Si}	n_{Fe}/n_{Si} by XPS	X_{NO} (max) (%)	T (X_{max}) (K)	$10^4 \frac{r(NO)}{Fe}$ (s^{-1})
	$FeCl_3$ introduction	Washing	Calcination ramp to 873 K							
Fe–Z(A)	CVD	1 liters/5 g	5 K/min[a]	5.4	0.92	0.065	0.027	73	603	4.1
Fe–Z(A, C_{10})	CVD	1 liters/5 g	10 K/min	5.2	0.88	0.063	—	67	603	4.0
Fe–Z(A, $C_{0.5}$)	CVD	1 liters/5 g	0.5 K/min	5.3	0.90	0.064	—	71	603	4.1
Fe–Z(A,W_{10}, $C_{0.5}$)	CVD	10 liters/5 g	0.5 K/min	5.0	0.84	0.060	0.039	74	603	4.5
Fe–Z(A, SSIE, *n*W)	SSIE	—	—	8.7	1.48	0.11	0.39	59	573	3.15
Fe–Z(B)	CVD	1 liters/5 g	5 K/min[a]	2.6	1.13	0.029	0.034	19	573–623	2.2

Note. Codes, preparation procedures, Fe content in bulk and external surface region (XPS) and reactivity in the SCR of NO by isobutane (for conditions see Fig. 1)—peak NO conversions with reaction temperatures required and normalized reaction rates at peak conversion.

[a] With predrying at 423 K (see text).

coefficient of iron on the basis of Lambert–Beer's law. Since the (dried/calcined) materials had contact with the ambient atmosphere during sample conditioning for the EXAFS measurements, there may be a systematic error due to adsorbed moisture, which should be, however, below $10\%_{rel}$. The results were confirmed by ICP analyses of representative samples. Also given in Table 1 are the bulk Fe/Si ratios.

For comparison with the present catalysts, results obtained with a Fe–ZSM-5 sample prepared by threefold aqueous ion exchange ("Fe–Z(Aq)"), the reactivity data of which was reported recently in (11), will be also cited in this paper. The iron content of the sample was 2.4 wt%.

Catalysis

The SCR of NO with isobutane was carried out in a catalytic microflow reactor at temperatures between 823 and 523 K. First, the catalyst (300 mg) was heated in flowing He to 823 K at 5 K/min and kept at this temperature for 1 h before the run was started at this temperature. A feed mixture of 1000 ppm NO, 1000 ppm isobutane, and 2% O_2 in He was charged to the catalyst at a flow rate of 220 ml/min, which results in a GHSV of 30,000 h^{-1}. For comparison with literature results, a mixture of 2000 ppm NO, 2000 ppm isobutane, and 3% O_2 in He was also employed, with the GHSV adjusted to 42,000 h^{-1} in this case (cf. (4, 6)). The composition of the effluent was analyzed by combination of gas chromatography (N_2, O_2; on a 5-A molecular sieve) and calibrated mass spectrometry (NO, CO, CO_2, O_2, H_2O, isobutane, NO_2). In this analysis scheme, it is difficult to distinguish between N_2O and CO_2, and NO_2 is indicated with low sensitivity due to its fragmentation behavior in the mass spectrometer. However, experiments in which photometric N_2O and/or NO/NO_2 analyzers were employed, on the basis of nondispersive IR photometry, ensured that these products did not form to any significant extent under our reaction conditions. This is supported by the fact that our analysis scheme rendered N balances of typically between 95 and 105%.

Catalyst Characterization

X-ray diffractograms were measured with a Siemens D-500 diffractometer using Cu $K\alpha$ irradiation. X-ray photoelectron spectra were obtained with a Leybold LH 10 spectrometer equipped with an EA 10/100 multichannel detector (Specs, Mg $K\alpha$ excitation, 10 kV, 20 mA). Elemental ratios in the XPS sampling region were evaluated from line intensity ratios using sensitivity factors given in (12).

IR spectra were recorded in diffuse reflection mode (DRIFT) using a Nicolet Protegé 460 FTIR spectrometer equipped with an MCT detector. The diffuse reflection attachment (Harrick) was in Praying Mantis geometry. The spectra were recorded as single-beam spectra at a resolution of 4 cm^{-1} averaging 1000 scans. The samples were dried and calcined in the cell in flowing argon or dry air with a 5 K/min temperature ramp to 873 K followed by a 1-h isothermal period. The spectra were recorded at 523 K and are reported in apparent absorption units obtained by dividing the measured spectra by background spectra (KBr) and taking the negative logarithm.

X-ray absorption spectra (Fe K edge at 7.112 keV) were measured at Hasylab E4 station (Hamburg) using a Si(111) double-crystal monochromator, which was detuned to 70% maximum intensity to exclude higher harmonics present in the X-ray beam. Absorption spectra $\mu(k)$ were measured in transmission mode using ion chambers with the sample at liquid nitrogen temperature. An iron metal foil was measured at the same time (between the second and a third ion chamber) for energy calibration. Samples were diluted with polyethylene, pressed into disks of suitable thickness and stored in ambient atmosphere. Data treatment was carried out using the software package WinXAS2.0 (13). For background subtraction and XANES normalization a linear polynomial was fitted to the preedge region and a third-order polynomial to the postedge region. A smooth atomic background, $\mu_0(k)$, was evaluated using cubic splines. The radial distribution function FT$[k^3\chi(k)]$ was obtained by Fourier transformation of the k^3-weighted experimental function $\chi(k) = (\mu(k) - \mu_0(k))/\mu_0(k)$ multiplied by a Bessel window. For the determination of structural parameters the FEFF7 analysis package (14) was used. To minimize the number of free parameters, equal backscatters were fitted with the same E_0-shift wherever possible and with a similar Debye–Waller factor by varying only the Debye temperature. For better discrimination between light and heavy scatterers (e.g., O, Si, and Fe), the spectra were fitted also after weighting by k^1. Additional support for the assignments derived was obtained in the fitting procedure, in particular from the imaginary part of the Fourier transformation.

Temperature-programmed reduction was carried out with a mixture containing 4.2 vol% H_2 in He (84 ml/min), with a 10 K/min temperature ramp between room temperature and 1073 K. The hydrogen content of the effluent was measured by a Hydros instrument (Fisher–Rosemount), which is based on catharometry. The samples were studied after calcination in air at 873 K. To ensure optimum conditions, sample amounts were chosen according to the Monti–Baiker criterion (15) unless stated otherwise.

The Mössbauer spectra were recorded with a constant-acceleration 4096 channels Mössbauer spectrometer (produced by Wissenschaftliche Elektronik GmbH, Starnberg/Germany) using a source of ^{57}Co in the chromium matrix with an activity of approximately 1 GBq. A proportional counter was used with a voltage of 1950 V to detect the spectra. The samples (300 mg) were placed in sealable cylindrical polyethylene sample compartments (inner diameter $d = 19$ mm) in a glove box. The measurement time was 6–8 days for each sample.

RESULTS

Catalysis

Figure 1 reports the temperature dependence of NO and isobutane conversions obtained with the Fe–ZSM-5 catalysts used in this study. Figure 1A shows conversion data of the reference preparation Fe–Z(A) measured under standard reaction conditions (I) and the conditions used by Chen and Sachtler (6) (II). The peak NO conversion achieved under standard conditions was 73%, and values of 71, 74, and 77% were found in repeated experiments. Changing the reaction conditions to those of (6) resulted in an upward shift of the conversion-temperature curve by 25 K, but only slight loss in peak NO conversion (69%, achieved at 623 K). In (6), peak NO conversions of 76% (at 623 K) were reported for (unpromoted) Fe–ZSM-5; i.e., the activity of our catalyst is only slightly below that reported by Sachtler's group.

In Fig. 1B, NO conversions measured under standard reaction conditions are compared for the remaining catalysts, which represent characteristic variations of the preparation route: variation of the matrix (Fe–Z(B)), of the $FeCl_3$ introduction method (Fe–Z(A, SSIE, *n*W)), and of the calcination and washing steps (Fe–Z(A, $C_{0.5}$), Fe–Z(A, W_{10}, $C_{0.5}$)). Also reported is an experiment with a physical mixture of α-Fe_2O_3 (5 wt% Fe) and H–ZSM-5(A). The isobutane conversions have been given only for those runs where the trend differs significantly from that shown in Fig. 1A for the standard preparation—Fe–Z(B) and the mechanical mixture α-Fe_2O_3/H–ZSM-5(A). In these cases, the isobutane conversion increases only gradually over the whole temperature range. Figure 1B shows that introduction of Fe species into H–ZSM-5 leads to higher NO conversions than the mix of Fe_2O_3 and zeolite. Among the catalysts containing intrazeolite iron, the only variation leading to a pronounced change in the SCR activity was that of the zeolite matrix: the NO conversions achieved with Fe–Z(B) remain below 20% while the remaining samples provide peak NO conversions ranging between 59 and 73%, but with slight differences in the catalytic behavior below the conversion maximum. Remarkably, the NO conversions achieved with Fe–Z(B) were even lower than those obtained with the mechanical mixture although the former sample was more active for the activation of isobutane. The last columns of Table 1 summarize the peak NO conversions and compare the catalysts on the basis of a normalized reaction rate, which relates the maximum reaction rate (mol NO/g_{cat} s) to the amount of iron present (mol Fe/g_{cat})). This "average activity" of the iron is almost identical for most samples but lower for those with $n_{Fe}/n_{Al} > 1$. With the Fe–ZSM-5 obtained by aqueous ion exchange (Fe–Z(Aq)), a peak NO conversion of 23% was obtained at 623 K (11), with an isobutane conversion curve very near that of the Fe_2O_3/H–ZSM-5 mixture. The normalized reaction rate (2.4×10^{-4} s^{-1}) is comparable to that of Fe–Z(B).

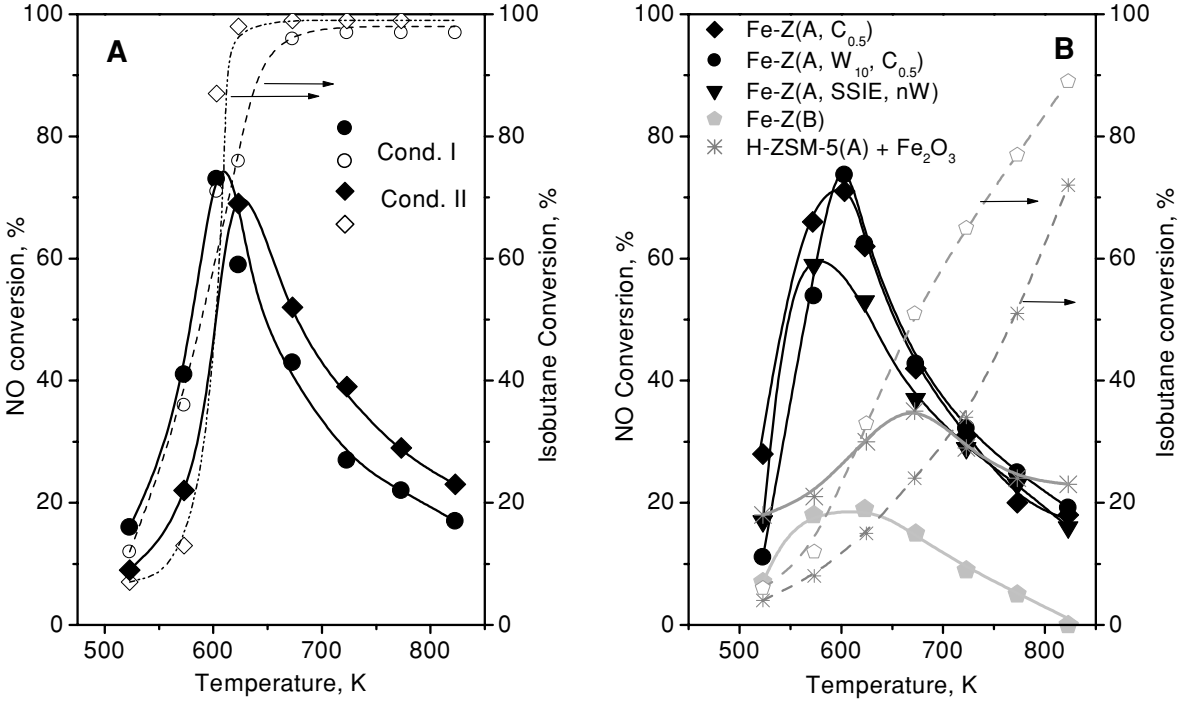

FIG. 1. Activity of Fe–ZSM-5 catalysts in the SCR of NO by isobutane. (Closed symbols) NO conversion; (open symbols) isobutane conversions. (A) Variation of reaction conditions. I: 1000 ppm NO, 1000 ppm isobutane, 2% O_2 in He, 30,000 h^{-1}. II: 2000 ppm NO, 2000 ppm isobutane, 3% O_2 in He, 42,000 h^{-1}. Catalyst, Fe–Z(A). (B) Variation of preparation details; reaction conditions I. For explanation of sample codes see Table 1.

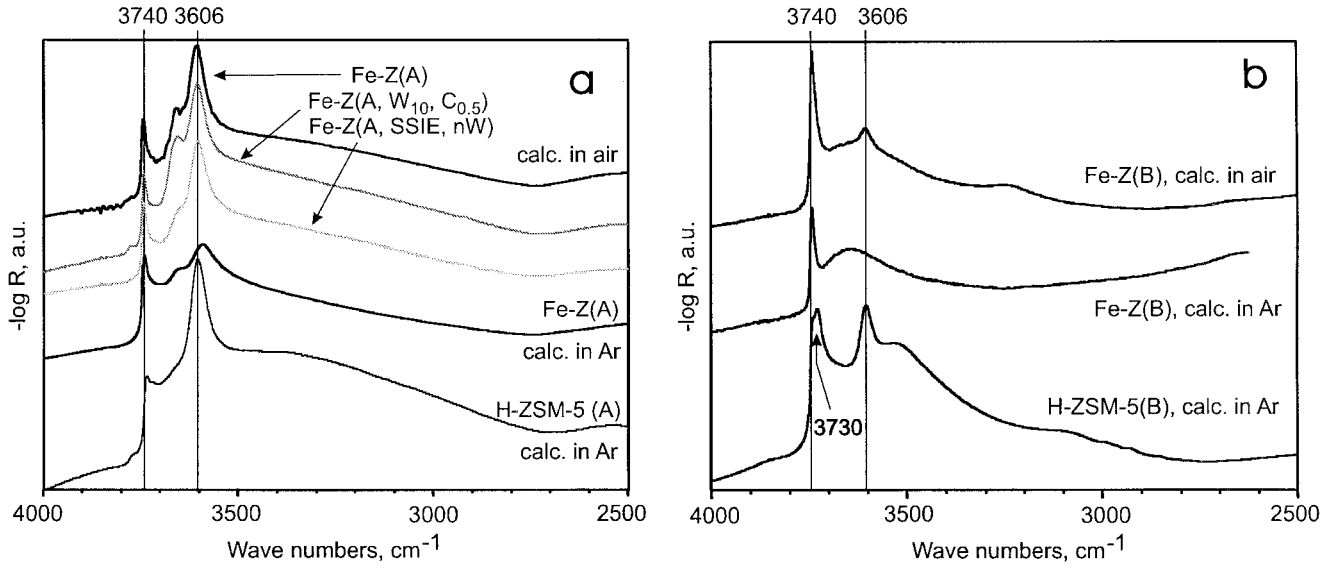

FIG. 2. DRIFT spectra of Fe–ZSM-5 prepared by CVD of $FeCl_3$ into different H–ZSM-5 materials. (a) Preparations based on H–ZSM-5(A); (b) preparation based on H–ZSM-5(B). (Black traces) Parent zeolite, samples after Fe introduction, washing, and dehydration by thermal treatment in Ar or by calcination in air at temperatures up to 873 K; (gray traces) Fe–Z(A, W_{10}, $C_{0.5}$) and Fe–Z(A, SSIE, nW) after calcination in air. For explanation of sample codes see Table 1.

Catalyst Characterization

DRIFTS. Figure 2 presents DRIFT spectra (OH region) of Fe–Z(A) and Fe–Z(B) at different stages of the preparation and compares them with the spectra of the parent zeolites. In addition, spectra obtained with some other samples are displayed in gray. The spectra have been normalized to the framework overtone vibrations between 1800 and 2000 cm^{-1}, which are not shown in the figure. From Fig. 2 it can be seen that there are pronounced differences between the two matrices: H–ZSM-5(A) exhibits an intense band typical of Brønsted OH groups at 3606 cm^{-1} (Fig. 2a), a weak signal at 3740 cm^{-1} (silanol groups), and a broad signal centered about 3250 cm^{-1} (interacting Brønsted OH groups). In contrast, H–ZSM-5(B) exhibits an intense signal of silanol groups and a weak signal of Brønsted OH groups (Fig. 2b). In addition, there is an intense signal at 3730 cm^{-1}, and a broad band centered at ≈3500 cm^{-1}, which can be assigned to silanol groups interacting with other atoms, e.g., in silanol nests (16).

A spectrum recorded with Fe–Z(A) after the chemical vapor deposition of $FeCl_3$ has been omitted because no comparable spectrum was measured with Fe–Z(B), for experimental reasons. In accordance with earlier results (6, 7), the signal of Brønsted OH groups disappeared completely after H–ZSM-5(A) had been loaded with $FeCl_3$. Figure 2 reports spectra measured after the washing step (including dehydration and thermal treatment in Ar). In this state, there was only a weak signal around 3600 cm^{-1}in Fe–Z(A), i.e., slightly shifted relative to the original band of the Brønsted sites, and an additional signal occurred at ≈3650 cm^{-1} (Fig. 2a). A signal in this wavenumber region was assigned to Fe–OH groups recently, and a particular interaction of these OH groups with the hydrocarbon reductant was observed (17). While we cannot exclude the possibility that Fe–OH groups contribute to the 3650 cm^{-1} band in our samples, we have seen no particular reactivity of the species represented by this signal in an *in situ* DRIFTS study with these catalysts (18). We therefore assign it to bridging OH groups on extraframework Al (16), which indicates that the thermal treatment has led to a slight dealumination of the framework. After calcination in air, the signal at 3606 cm^{-1} was restored to a considerable extent, which can be estimated to be >50% of the original site density from a comparison with the spectrum of the parent zeolite. The signal of interacting Brønsted sites (broad feature centered around 3250 cm^{-1}) remained suppressed. In Fe–Z(B), the signal of Brønsted sites was not restored at all after washing and thermal treatment in Ar, and it reappeared only to a small extent even after calcination in air (Fig. 2b). Remarkably, the band attributed to silanol groups in silanol nests (3730 cm^{-1}) also disappeared by the interaction with $FeCl_3$, and it reappeared neither after washing nor after calcination in air. The band of free silanol groups (3740 cm^{-1}) was somewhat attenuated after washing but was completely restored after calcination in air.

The spectra of Fe–Z(A, W_{10}, $C_{0.5}$) and of Fe–Z(A, SSIE, nW) are very similar to that of Fe–Z(A), except for a weaker signal of extralattice Al species in the preparation by solid-state ion exchange, where the washing step was omitted. Possibly, the dealumination occurred largely on the final calcination of the dried samples.

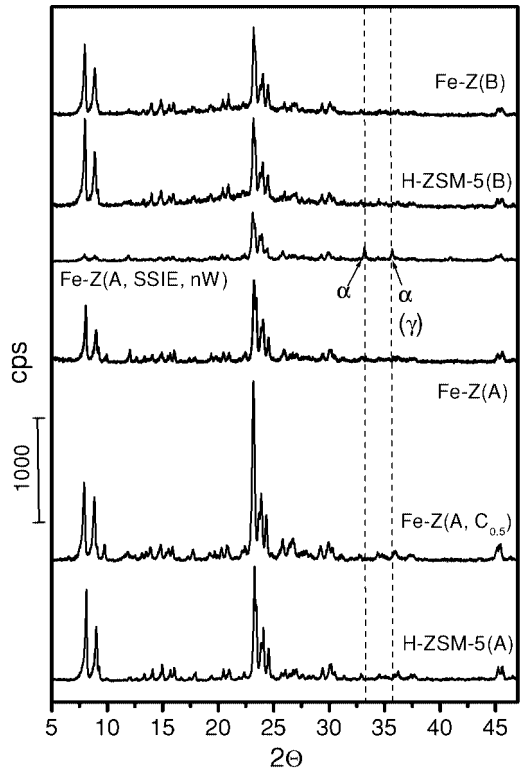

FIG. 3. X-ray diffractograms of parent zeolites (A) and (B) and Fe–ZSM-5 materials prepared from them. Main reflectances of α- and γ-Fe_2O_3 are indicated by broken lines. For explanation of sample codes see Table 1.

For Fe–Z(A) and Fe–Z(B), similar measurements are available also for the state after catalysis (taken *in situ* at 523 K (18)). However, there the signals of the Brønsted sites are strongly attenuated by interaction with coke deposits. In the case of Fe–Z(Aq), a FTIR spectrum obtained after calcination in air showed an intense signal of Brønsted sites despite the rather high Fe content; its relative intensity (related to the band at 1870 cm^{-1}) was about one-third smaller than that in the parent H–ZSM-5(A) (19).

XRD. Figure 3 compares the X-ray diffractograms of several Fe–ZSM-5 preparations with those of the parent zeolites H–ZSM-5(A) and H–ZSM-5(B). Positions at which strong reflectances of α-Fe_2O_3 and γ-Fe_2O_3 are expected are indicated by dotted lines. All samples exhibit the typical diffractograms of the MFI framework. The course of the baseline indicates that there is some amorphous material in H–ZSM-5(B), but the diffractogram shows that the abundance of lattice defects in this sample has not led to extensive framework damage. This conclusion is also supported by inspection of the IR framework vibrations at 460 and 560 cm^{-1} (19). In Fe–Z(A), Fe–Z(A, $C_{0.5}$), and Fe–Z(B), there are no indications of α-Fe_2O_3 or any other Fe oxide phase. On the other hand, reflectances at $2\Theta = 33.2$ and 35.7° indicate the presence of crystalline α-Fe_2O_3 in Fe–Z(A, SSIE, *n*W). The latter signal may also arise from γ-Fe_2O_3. In the iron-containing samples, the ZSM-5 reflectances at $2\Theta = 8.9$ and 8.0° are attenuated relative to the main signals around $2\Theta = 24°$. The effect is strongest in Fe–Z(A, SSIE, *n*W), well visible Fe–Z(A, $C_{0.5}$) and Fe–Z(A), but rather weak in Fe–Z(B). Such changes in the intensity ratios between reflectances of the zeolite host indicate the introduction of heavy scatterers (Fe) into the pore system.

XPS. Fe/Si atomic ratios in the external surface region are compared with Fe/Si bulk ratios in Table 1. The Fe $2p_{3/2}$ binding energies ranged from 710.6 to 710.8 eV (related to Si 2p = 103.0 eV), and the signal shape indicated Fe^{3+} as the majority oxidation state. In the catalyst prepared by SSIE, the Fe/Si atomic ratio derived from XPS was significantly larger than the bulk ratio while a different trend was obtained with samples prepared by CVD. It should be noted, however, that the determination of Fe intensities is rather inaccurate with these samples because of the large signal width (satellites included) and considerable uncertainty about the course of the baseline in this region. From the data it can, however, be concluded that Fe is well dispersed over the zeolite crystal by the sublimation procedure while a surface enrichment remained after the SSIE preparation. It is possible that the Fe_2O_3 crystals detected by XRD are located on the external surface. Before catalysis, the surface region of Fe–Z(A, SSIE, *n*W) contained significant amounts of chlorine, which was almost completely removed during the catalytic run.

X-ray absorption. Figure 4 shows the near-edge regions of the X-ray absorption spectra taken from the samples under study and compares them with those of reference materials: α- and γ-Fe_2O_3, and Fe-beta. In Fig. 5, the absolute part of the Fourier transformed EXAFS spectra of these samples (except Fe-beta) are presented. These spectra have been analyzed, and the results are summarized in Tables 2 and 3 while Fig. 6 gives a graphical representation for some of the fits.

In the XANES spectra shown in Fig. 4, relevant information can be drawn from the width and the height of the preedge peak A, from the edge position, and from the existence of multiple scattering features beyond the edge, which are labeled C and D. The edge positions of all catalyst samples agrees with those of the reference iron oxides, which indicates that iron is predominantly in the +3 oxidation state.

The preedge absorption peak (A) in Fe–K XANES arises from a 1s → 3d transition, which is forbidden in octahedral coordinations (O_h) but occurs in coordinations without inversion center (distorted octahedral, tetrahedral). It is known from high-resolution measurements (20) that the preedge peak is narrower and more intense with Fe^{3+} in tetrahedral coordination (T_d). This is confirmed by comparison of the A feature in the reference iron oxides: it is

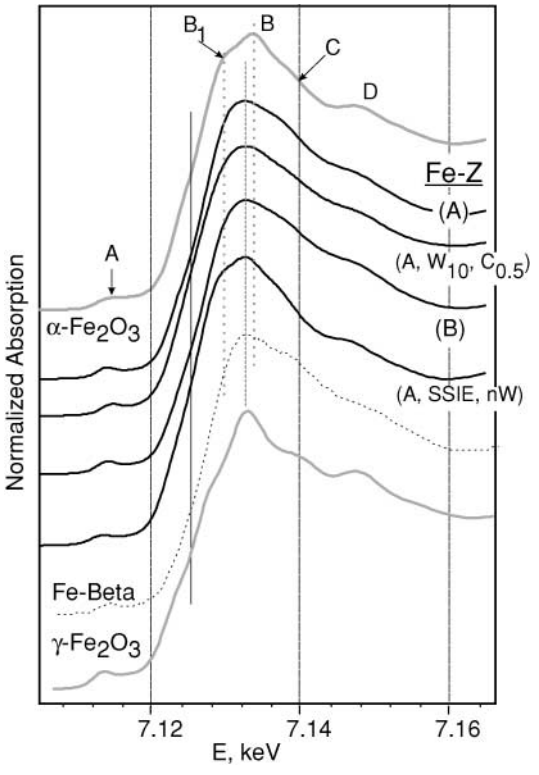

FIG. 4. XANES of iron oxides, Fe-beta (references), and Fe–ZSM-5 catalysts of different preparation, all after use in catalysis. For interpretation of features A through D see text; for interpretation of sample codes see Table 1. Fe content of Fe-beta, 1.6 wt%.

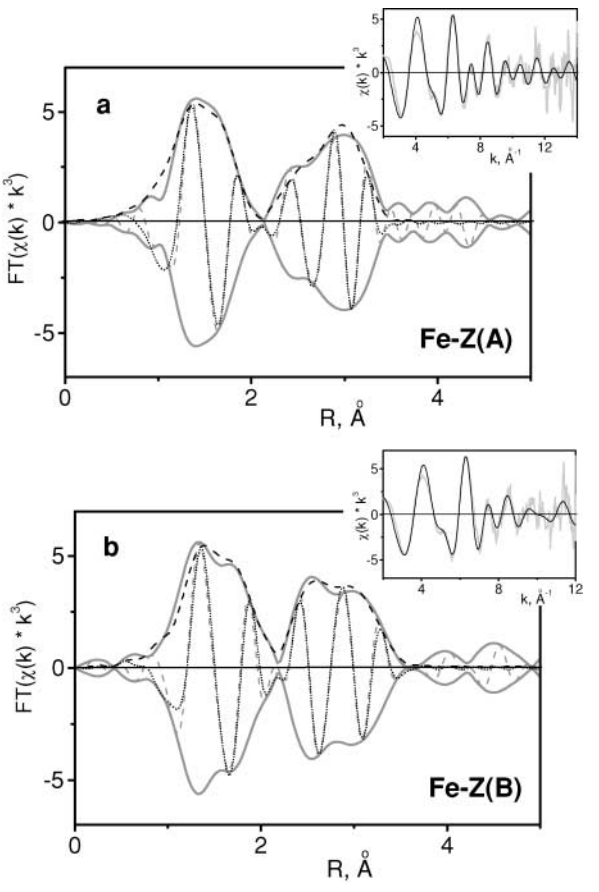

FIG. 6. Examples for fits obtained for EXAFS spectra of Fe–ZSM-5 catalysts (first and second spheres fitted). For fit parameters see Tables 2–4.

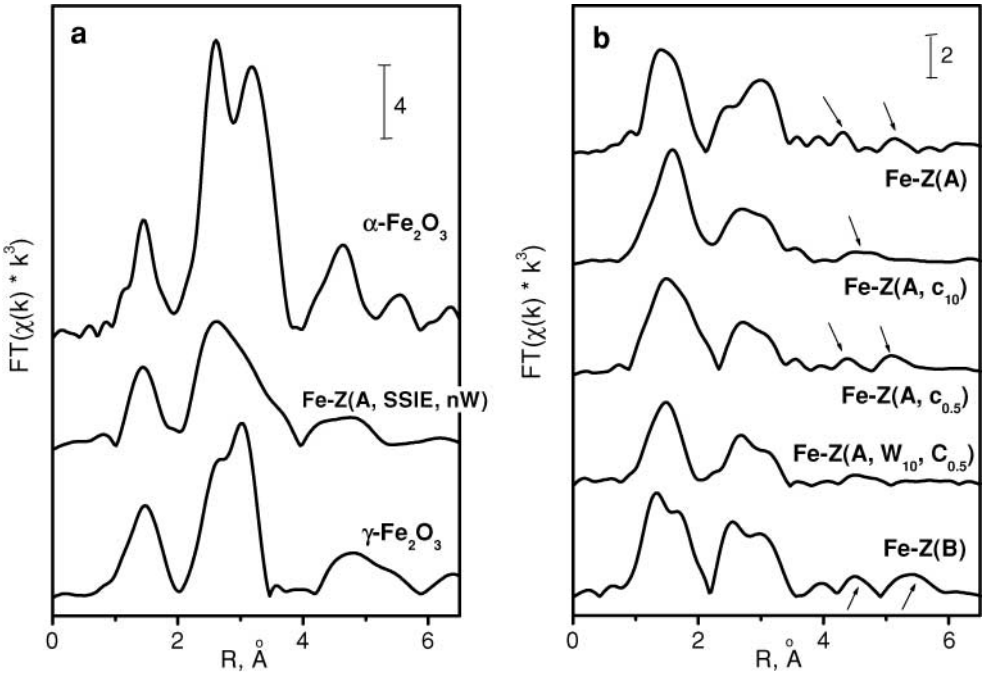

FIG. 5. EXAFS spectra (real part of Fourier transform of k^3-weighted spectra, $k = 2$–15 Å^{-1}) of iron oxides and Fe–ZSM-5 catalysts after use in catalysis. Possible scattering features from higher shells marked by arrows in panel b. For explanation of sample codes see Table 1.

less intense and broader with α-Fe_2O_3 (Fe^{3+} in distorted O_h coordination) than with γ-Fe_2O_3 (50% of Fe^{3+} in T_d and in distorted O_h coordination). Among the catalysts, sample Fe–Z(A, SSIE, *n*W) strongly resembles α-Fe_2O_3 with respect to the preedge peak, while in the remaining spectra, the latter is narrower. This indicates the presence of Fe^{3+} ions in tetrahedral coordination in these catalysts. However, since the intensity of the preedge peak is lower than in γ-Fe_2O_3, the tetrahedrally coordinated Fe ions probably amount to less than 50% of the total iron present in the samples.

The position of the absorption maximum B as well as of the features C and D, which indicate the presence of order beyond the first coordination sphere, differ slightly between the reference oxides. The most prominent difference is, however, the existence of a pronounced shoulder at B (B_1) in α-Fe_2O_3, which is practically absent in γ-Fe_2O_3. The spectrum of Fe–Z(A, SSIE, *n*W) resembles that of α-Fe_2O_3 also with respect to this shoulder. Indeed, the presence of α-Fe_2O_3 in this sample was also confirmed by XRD (*vide supra*) and EXAFS (*vide infra*). On the other hand, the XANES of the reference Fe-beta sample, for which the analysis of the EXAFS region indicated the coexistence of γ-Fe_2O_3 aggregates with well-dispersed Fe^{3+} species (21), is much closer to that of γ-Fe_2O_3 in the vicinity of the maximum B. The XANES of the remaining catalysts is intermediate in this region. While it does not exhibit a distinct shoulder, it is clearly broader than that of Fe-beta. This might arise from the presence of a completely different coordination geometry. However, in all these spectra, the scattering feature D indicating the existence of order in higher coordination spheres is clearly observed, and this order should be reflected in the shape of the B feature. Since the shape is between those of materials containing aggregates with the short-range order of one of the iron oxides, it may be concluded that species with the short-range order of both iron oxides coexist in these materials.

Figure 5 presents results of the EXAFS study of Fe–ZSM-5 samples after use in catalysis and of the reference iron oxides (Fourier transform (absolute part) of the k^3-weighted spectra). From Fig. 5a, it is obvious that the differences in the structure of these oxides can be well distinguished by EXAFS in particular in the region of the second shell, which exhibits two peaks: in α-Fe_2O_3, the second maximum appears at a different distance and is broader than in the case of γ-Fe_2O_3. The spectrum of Fe–Z(A, SSIE, *n*W) resembles that of α-Fe_2O_3 to some extent, but the maximum at ~3.2 Å (uncorrected) appears only as a shoulder. Although the relative intensity of the second shell is much smaller than in the case of the pure oxides, higher coordination spheres are clearly visible in the spectrum. With the other samples (Fig. 5b), the intensity of the second shell is significantly smaller. These spectra do not differ very much from each other except for some intensity variations between the first and second shells and the extent to which signals at higher distances can be detected. The latter are always weak but significant in some samples (Fe–Z(A, $C_{0.5}$), Fe–Z(B)) while doubtful in other cases (Fe–Z(A), Fe–Z(A, C_{10}), Fe–Z(A, W_{10}, $C_{0.5}$)).

TABLE 2

Fit Results Obtained for Reference Materials from EXAFS Spectra Reported in Fig. 5

Material	No.	Element	*R* (Å)	CN	$10^3\ \sigma^2$ (Å^{-2})//E_0 (eV)
α-Fe_2O_3					
	1	O	1.94	4.0	6.2//−3.8
	2	O	2.13	2.0	6.5//−1.3
	3	Fe	2.95	2.6	2.1//−2.5
	4	Fe	3.34	2.9	3.2//−2.5
	5	Fe	3.68	6.0	3.4//−2.5
	6	O	3.76	3.0	7.4//−1.45
γ-Fe_2O_3					
	1	O	1.88	2.2	4.7//−0.6
	2	O	2.00	2.3	5.0//−0.6
	3	Fe	2.97	1.9	5.9//−4.8
	4	Fe	3.42	6.5	6.4//−4.8

Fit results obtained from the spectra shown in Fig. 5, and additionally from spectra taken after mere calcination in synthetic air, are given in Tables 2 and 3. Those for α-Fe_2O_3 and Fe–Z(A, SSIE, *n*W) were obtained by cluster fits, which started from the real α-Fe_2O_3 structure (22) and included multiple scattering paths up to four scattering events. For α-Fe_2O_3, only the major scattering channels are reported; an additional Fe coordination at ≈2.9 Å and an oxygen coordination ≈3.8 Å, which yield only small contributions, have been omitted in the table. The spectrum of γ-Fe_2O_3 was fitted without consideration of multiple scattering. Despite this slight methodical difference, it can be derived from the comparison of the references that γ-Fe_2O_3 has lower distances and coordination numbers (CNs) in the first (O) shell, which results from the presence of tetrahedrally coordinated Fe. Among the Fe coordinations, the first one (≈2.95 Å) is practically identical in the two oxides while the second one is at a lower distance in α-Fe_2O_3. Notably, the third Fe coordination, which is quite pronounced in α-Fe_2O_3, is missing in γ-Fe_2O_3.

Among the catalysts, Fe–Z(A, SSIE, *n*W) indeed contains O and Fe neighbors at distances similar to those in α-Fe_2O_3 (Table 3). In particular, the distances beyond the first shell agree very well. Differences in the first Fe–O distances from those in the oxide and the smaller CNs of the Fe–Fe coordinations indicate that there is an additional Fe species in the sample, with a structure that does not contribute to the higher Fe coordinations and that has Fe–O distances other

TABLE 3

Fit Results Obtained for Catalysts (Reaction Condition I) from EXAFS Spectra Reported in Fig. 5

Catalyst	No.	Element	R (Å)	CN	$10^3\ \sigma^2$ (Å^{-2})//E_0 (eV)
Fe–Z(A, SSIE, nW) after preparation (after catalysis)					
	1	O	1.96 (1.99)	2.8 (3.4)	5.5//1.7 (2.2//0.2)
	2	O[a]	2.08 (2.14)	3.3 (1.6)	5.8//1.7 (2.3//0.2)
	3	Fe	2.96 (2.95)	2.1 (1.4)	5.6//−2.65 (0.9//−4.45)
	4	Fe	3.35 (3.34)	2.8 (1.4)	5.6//−2.65 (0.9//−4.45)
	5	Fe	3.69 (3.68)	2.8 (0.7)	5.6//−2.6 (0.9//−4.45)
	6	O	−(3.76)	−(5.3)	−(2.6//0.2)
Fe–Z(A) after calcination in syn. air (after catalysis, cf. Fig. 6)					
	1	O	1.93 (1.87)	2.0 (2.4)	4.0//1.4 (6.8//−0.1)
	2	O	2.07 (2.02)	3.7 (3.0)	4.4//1.4 (5.8//−0.1)
	3	Fe	2.98 (2.95)	0.5 (0.6)	1.8//−7.25 (7.65//−6.6)
	4	Fe	3.37 (3.40)	0.8 (2.2)	2.0//−7.25 (6.2//−6.6)

Fit Results Obtained for Catalysts (Reaction Condition II) from EXAFS Spectra Reported in Fig. 5[a]

Catalyst	No.	Element	R (Å)	CN	$10^3\ \sigma^2$ (Å^{-2})//E_0 (eV)
Fe–Z(A, C_{10}) after catalysis					
	1	O	1.965	2	3//−9.0
	2	O	2.10	2	1//−9.1
	3	Fe	2.95	0.4	0.03//−7.4
	4	Fe	3.37	0.55	0.03//−7.4
Fe–Z(A, $C_{0.5}$) after catalysis					
	1	O	1.95	2	3//−9.1
	2	O	2.09	2	1//−9.6
	3	Fe	3.00	0.4	0.03//−6.5
	4	Fe	3.38	0.45	0.03//−6.5
Fe–Z(A, W_{10}, $C_{0.5}$) after catalysis (cf. Fig. 6)					
	1	O	1.89	2.0	8.2//−2.8
	2	O	2.02	2.5	8.9//−2.1
	3	Fe	3.02	1.6	11.3//−0.85
	4	Fe	3.41	0.85	6.4//1.5
Fe–Z(B) after calcination in syn. air (after catalysis, cf. Fig. 6)					
	1	O	1.87 (1.90)	2.1 (2.5)	6.3//−2.45 (4.8//3.1)
	2	O	2.02 (2.06)	3.0 (2.85)	7.0// − 2.45 (3.45//3.1)
	3	Fe	2.96 (2.97)	0.5 (1.8)	2.9//−10.9 (10.95//−2.6)
	4	Fe	3.36 (3.44)	0.7 (3.1)	3.1//−10.9 (10.8//−2.6)

[a] Due to uncertainties inherent in the analysis of the first shell (see text), no attempt was made to extract the possible contribution of Cl from the spectrum measured after preparation (cf. XPS results).

than the oxide. In α-Fe_2O_3, the CNs of the Fe neighbors at 2.95 and 3.34 Å are close while that of the next coordination (3.68 Å) is higher. This trend is reproduced for the catalyst prepared by SSIE except for the outer Fe neighbor: its CN was found to be equal or smaller—despite some differences in the fits for Fe–Z(A, SSIE, nW) after calcination or after catalysis. Such amplitude decay indicates the presence of very small particles. On the other hand, there are rather intense scattering contributions still at higher R values, which arise from larger particles. As a result it can be concluded that in Fe–Z(A, SSIE, nW), highly disperse species coexist with small clusters and with larger crystallites exhibiting α-Fe_2O_3 short-range order.

The remaining catalysts differ from Fe–Z(A, SSIE, nW) in the Fe–O bond distances, which are consistently smaller than those in α-Fe_2O_3 (despite some differences between the individual samples) and in the absence of a significant scattering contribution at 3.68 Å. The sum of the first O neighbors was found between 4 and 6, which seems to indicate the presence of tetrahedrally coordinated Fe. However, in view of the limited accuracy of coordination numbers, we think that the latter is inferred only by a combination of a low sum of coordination numbers *and* low Fe–O distances (e.g., in γ-Fe_2O_3, Table 2, and Fe–Z(A, W_{10}, $C_{0.5}$) and Fe–Z(B), Table 3). The Fe–Fe CNs were <1 in most cases, which means that there has to be the additional contribution of an iron species without iron neighbors. In some samples (Fe–Z(A), Fe–Z(B) after catalysis) the CN of the outer Fe neighbor was significantly larger than that of the inner one. The distance of the former (3.36–3.44 Å) was

consistently longer than that in α-Fe_2O_3 (3.35 Å) and eventually identical with that in γ-Fe_2O_3 (3.42 Å). Remarkably, in some cases, a satisfactory fit of the spectrum was obtained only with unrealistic, strongly negative E_0 values or with too-small Debye–Waller factors for the Fe neighbors. This indicates that the model assumed was not really adequate, most likely due to the presence of an additional scatterer, the location of which could not be traced, however, on the basis of the present data.

These observations lead to the conclusion that the second shell indeed arises from a mixture of clusters with the short-range order of the two iron oxides. Indeed, where the distance of the second Fe–Fe shell approached that known from γ-Fe_2O_3 (Fe–Z(A), Fe–Z(B) after catalysis), its CN took a rather large value, as known from γ-Fe_2O_3 (Table 2). Where order could be observed still at higher R, the larger crystallites should have the structure of γ-Fe_2O_3, since the absence of any significant contribution at 3.68 Å shows that the short-range order of α-Fe_2O_3 is realized only in very small clusters (oligomers). In summary, EXAFS indicates the presence of iron in three types of species—monomeric, oligomeric, and aggregates (crystallites) with the short-range order of α- and of γ-Fe_2O_3, where the former occurs only in the oligomer moiety. From the FT spectra shown in Fig. 5b, it can be derived that significant amounts of crystallites are present in Fe–Z(A, $C_{0.5}$) and Fe–Z(B). The situation is less clear with Fe–Z(A), Fe–Z(A, C_{10}), and Fe–Z(A, W_{10}, $C_{0.5}$).

The EXAFS analysis of our Fe–ZSM-5 catalysts differs significantly from results published earlier in the literature. Thus, we could not find a Fe–Fe coordination at ≈2.5 Å, as was reported in (9) and discussed in (7, 8). On the other hand, a comparison with spectra published earlier (7–10, 23) shows that our spectra (i.e., our materials) are indeed different. From their FT (Fig. 5), it is quite obvious that there is a scatterer beyond the one at ≈3 Å (≈2.5 Å uncorrected), which is the only one detected in the earlier work. This scatterer could be readily identfied as iron. In (8, 23), the first shell was fitted by three oxygen coordinations, with the outer one at distances of 2.15–2.27 (8) and 2.48 Å (7, 23). In our spectra, fits with three oxygen coordinations in the first shell were often not stable, or they did not result in improvements of the fit quality that would have allowed a claim of significance for the third coordination (at ≈2.45 Å).

In Fe–Z(Aq), no Fe neighbors were detected in the Fe coordination sphere by EXAFS (11, 21).

Temperature-programmed reduction. Figure 7 shows the TPR profiles of the Fe–ZSM-5 samples and compares them with TPR profiles of the reference oxides α-Fe_2O_3 and γ-Fe_2O_3. The latter were measured in physical mixtures of the oxides with H–ZSM-5(A) (5 wt% Fe); in the case of γ-Fe_2O_3, the TPR curve was also recorded with the pure oxide (curve e′, gray). The hydrogen consumption signals are related to the Fe contents of the samples (cf. Table 1);

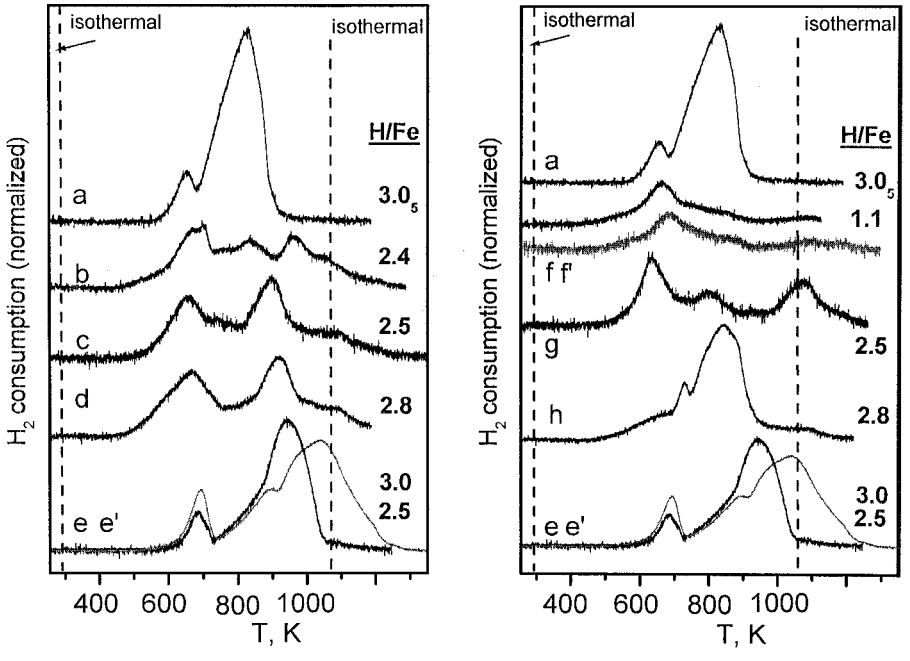

FIG. 7. TPR profiles of iron oxides and Fe–ZSM-5 catalysts. H_2 consumption normalized to Fe content in the samples. (a) α-Fe_2O_3 (5 wt% Fe)/H–ZSM-5; (b) Fe–Z(A); (c) Fe–Z(A, C_{10}); (d) Fe–Z(A, $C_{0.5}$); (e) γ-Fe_2O_3 (5 wt% Fe)/H–ZSM-5; (e′) γ-Fe_2O_3; (f) Fe–Z(A, W_{10}, $C_{0.5}$); (f′) as for f, sample previously used for Mössbauer spectroscopy; (g) Fe–Z(B); (h) Fe–Z(A, SSIE, nW). For explanation of sample codes see Table 1.

hence, the integrals over the curves are proportional to the total reduction degree achieved (H/Fe).

In the literature, the TPR curves of Fe catalysts are often discussed by reference to that of α-Fe_2O_3 (6, 9, 24, 25). The profile shown for α-Fe_2O_3 (mixed with H–ZSM-5) in Fig. 7 agrees well with those given in the literature. The trace obtained for γ-Fe_2O_3/H–ZSM-5 is rather similar, but the peak temperature of the high-temperature signal is shifted upward by ≈120 K. It is, however, not clear whether this shift reflects the structural differences between these oxides, because the reduction kinetics of iron oxides is also influenced by particle size and morphology, defect density, and so forth (26). Moreover, by comparing the results for pure γ-Fe_2O_3 with its mechanical mixture with H–ZSM-5, a further upward shift was found for the pure oxide. The H/Fe values measured with the oxides were between 2.5 and 3.05 (3.0 expected), which indicates a limited accuracy of the reduction degrees obtained. The ratio between hydrogen consumption in the high- and low-temperature signals was between 8 and 9, as expected for the reduction sequence $Fe_2O_3 \rightarrow Fe_3O_4 \rightarrow Fe(0)$. For the detection of intrazeolite iron oxide aggregates, which might be located in mesopores created by particle growth, the Fe_2O_3 references are of limited value since prediction of the influence of the surrounding zeolite matrix is not straightforward. Due to the small cluster sizes possible in such locations, the peak reduction temperatures should be decreased. On the other hand, the higher water partial pressures, which arise from delayed water removal from the surrounding microporous network, should tend to increase the reduction temperatures.

The TPR profiles of the catalysts are rather complicated, with the exception of the samples Fe–Z(A, SSIE, *n*W) (Fig. 7, trace h) and Fe–Z(A, W_{10}, $C_{0.5}$) (traces f and f′). The TPR profile of Fe–Z(Aq) (27) was quite similar to the latter, but the main peak, at 665 K, had a strong shoulder at lower temperature (523 K), and a significant feature appeared around 823 K (H/Fe = 1.8). It can be seen from Fig. 7 that there is a low-temperature peak between 660 and 680 K in all Fe–ZSM-5 catalysts except Fe–Z(B), where it is shifted to 635 K, and Fe–Z(A, SSIE, *n*W), where only a shoulder is present in this region. Beyond this peak, numerous maxima or shoulders occur at different temperatures, e.g., at 725 K (Fe–Z(A, SSIE, *n*W)), 805 K (Fe–Z(B)), 835–845 K (Fe–Z(A), Fe–Z(A, SSIE, *n*W)), 895–925 K (Fe–Z(A, C_{10}), Fe–Z(A, $C_{0.5}$)), 965 K (Fe–Z(A)), 1045 K (all but Fe–Z(B), Fe–Z(A, SSIE, *n*W)), and 1075 K (Fe–Z(B)). The profile of Fe–Z(A, SSIE, *n*W) closely resembles that of the α-Fe_2O_3/H–ZSM-5 mixture, but the low-temperature peak of the latter is smeared out as a shoulder and a new low-temperature peak appears at 725 K. The ratio between hydrogen consumption in the high- and low-temperature signals amounts to 3.5. The large main peak at 845 K with its shoulder around 650 K certainly shows the presence of α-Fe_2O_3 aggregates near and on the external zeolite surface, as already indicated by XPS and XRD. The modified profile shape at low temperatures may arise from additional, well-dispersed Fe species.

The remaining catalysts except Fe–Z(A, W_{10}, $C_{0.5}$) also exhibit various features beyond the low-temperature signal and high overall hydrogen consumptions (H/Fe between 2.4 and 2.8). The ratio between hydrogen consumption in the high- and low-temperature signals is between 1.3 and 1.6. Although some of these peaks appear at temperatures similar to those in the reference oxides, their assignment as extrazeolite oxide aggregates would be in conflict with the XPS results: unlike in Fe–Z(A, SSIE, *n*W), no surface enrichment of iron was found in catalysts prepared by CVD. Remarkably, the variation of the calcination regime did not change the TPR profiles to any significant extent (Fig. 7, curves c and d). Sample Fe–Z(A), however, which was calcined at an intermediate rate, yielded a much more complicated profile (trace b). This sample originated from another batch of the preparation, and the differences arise most likely from slight variations in the washing process, which has a large influence on the Fe speciation: when the washing is strongly extended, the signals assigned to clustered phases are strongly suppressed (cf. traces f and f′), as was shown earlier in the literature (6, 7).

The H/Fe ratios should permit evaluation of the amount of Fe species on cation sites, and the ratio between hydrogen consumption in the high- and low-temperature signals should reflect their amount qualitatively. Isolated Fe^{3+} is known to be reduced to Fe^{2+} at low temperatures while further reduction to Fe(0) occurs only at temperatures well above those employed in this study (28, 29). A single low-temperature peak and a H/Fe ratio of 1, however, have also been considered to indicate the predominant presence of the binuclear Fe–O–Fe site (6). Generally, a high ratio of hydrogen consumption between high- and low-temperature peaks (ca. 8) shows the presence of crystalline iron oxide phases. In disperse, intrazeolite phases all Fe^{3+} ions should be first reduced to Fe^{2+}(H/Fe = 1), but their further fate should depend on their relation to the cation sites available: those not stabilized by a framework charge should be reducible to the metal. For binuclear complexes with 2, 1, or no Fe ion on cation sites, this would result in H/Fe ratios between high- and low-temperature peaks of 0, 1, and 2, respectively, but a multitude of intermediate values will be found if clusters of higher nuclearity are present. On this basis, Fe–Z(A, W_{10}, $C_{0.5}$) and Fe–Z(A, SSIE, *n*W) may be differentiated from the rest of the samples, which appear to be similar to each other. For Fe–Z(A, W_{10}, $C_{0.5}$), an experimental H/Fe value of 1.1 is given in Fig. 7, but this is probably low since the run was finished early. From a reproduction experiment (f′), which was of limited general accuracy due to violation of the Monti–Baiker criterion

(*vide infra*), it may be estimated that about 10% of the area was lost in trace f; i.e., H/Fe should amount to 1.2–1.3. According to that, the majority of Fe ions should be on cation sites, either isolated or paired. Fe–Z(A, SSIE, *n*W) does not differ from the remaining catalysts in the H/Fe ratio, but the higher ratio of hydrogen consumption in high- and low-temperature signals (3.5) suggests the coexistence of crystalline oxide aggregates and structures of high dispersion. According to this criterion, the ratio of 1.3–1.6 found with the remaining catalysts indicates a significant clustering at a generally high level of dispersion. The differences between the individual TPR traces suggest a complex structure of the iron phase, with significant differences between Fe–Z(A), Fe–Z(B), and Fe–Z(A, $C_{0.5}$) or Fe–Z(A, C_{10}). Most likely, several different Fe species coexist in all these samples.

Mössbauer spectroscopy. Figure 8 shows Mössbauer spectra of four Fe–ZSM-5 catalysts measured after catalytic runs. The catalysts studied represent the variation of the calcination conditions (Fe–Z(A, C_{10}), Fe–Z(A, $C_{0.5}$)), of the washing intensity (Fe–Z(A, $C_{0.5}$), Fe–Z(A, W_{10},$C_{0.5}$)), and, with some approximation, of the matrix (Fe–Z(A, C_{10}), Fe–Z(B), the latter calcined at 5 K/min). The spectra are very complex, and it is clear without any numerical analysis that several doublet and sextet signals are superimposed in them. The different linewidths of the sextet lines (compare Figs. 8a and 8b or 8d) implies that different sextet states may contribute to the spectral shapes. Generally, the sextet signals are broader in the case of catalysts calcined with a low-temperature gradient (Figs. 8b and 8d). The fit lines indicated are the result of spectral simulations performed with a standard least-squares routine (30). Two or three doublets and three or four sextets were required to arrive at the fit lines given. Details of this analysis and possible assignments, which are, however, subject to considerable uncertainty, are given in (31).

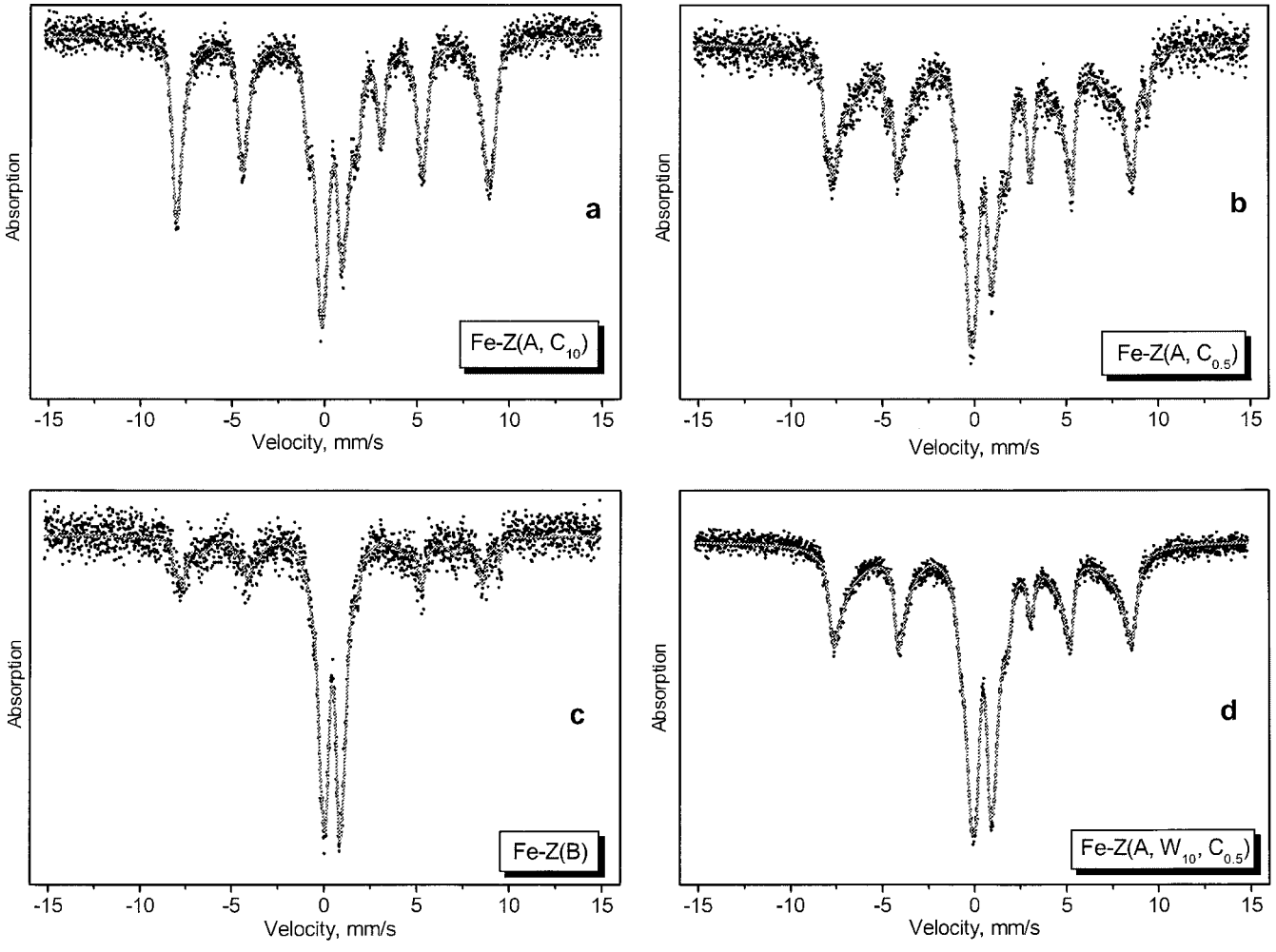

FIG. 8. Mössbauer spectra of Fe–ZSM-5 catalysts after use in catalysis. For explanation of sample codes see Table 1. The interpolation lines indicate results from a numerical analysis presented elsewhere (30, 31).

From the spectra, it may be deduced that in all catalysts prepared with matrix H–ZSM-5(A), a significant amount of different aggregates is present irrespective of the washing and calcination conditions (Figs. 8a, 8b, and 8d), while the aggregation is less intense in matrix B (Fig. 8c), where, in addition, the iron content is lower. Most of these signals, including the sextets, were also present in spectra measured at room temperature (32). The spectra measured with matrix A are similar on the whole although there are differences in detail. The doublets arise from Fe(III) in different octahedral coordinations (30, 31). Remarkably, a doublet component indicative of octrahedral Fe(II) (5–10% of the total signal area) is quite obvious at ≈3.5 mm/s. The contribution of the sextet signals to the total signal area was found to be between 55 and 65% (31, 32), and in room temperature spectra between 48 and 58% (32). The spectral parameters of the sextets indicate the formation of both γ- and α-Fe_2O_3 aggregates. The width of the signals implies that the size of the majority of aggregates is well below the size of the Weiss domains (superparamagnetic particles), which is also supported by the hyperfine field parameters found (30, 31).

In Fe–Z(B), the area of sextet signals was only 37% of the total signal area (at room temperature it was 32% (30–32)). This indicates that the quantity of large aggregates was much smaller in this material with Fe/Al > 1 than in those described above. No Fe(II) was detected in Fe–Z(B). Among the sextets were contributions of both iron oxides and a unidentified structure (30, 31).

It should be noted, however, that the contributions to the total signal area, which are cited above, do not necessarily reflect the abundance of the aggregated Fe species observed correctly. On the one hand, the total amount of clustered iron may well be larger because in very small clusters (oligomers) the thermal energy will outweigh the spin coupling even at 78 K: according to (33), temperatures <1 K are required to get magnetically split signals from 2-nm Fe oxide clusters. On the other hand, the Debye temperature of iron oxide aggregates should be significantly higher that of single ions on cation sites or oligomers (34). Hence, the contribution of small entities (isolated of paired sites) may be strongly underestimated. It is difficult to predict to which extent and in which direction the real distributions of phases will deviate from those reported in Fig. 8.

DISCUSSION

The characterization of Fe–ZSM-5 catalysts by various techniques rendered some general conclusions, but also unexpected contradictions. EXAFS, TPR, and Mössbauer spectroscopy all indicate that clustered phases are formed along with well-dispersed iron when Fe–ZSM-5 is prepared via CVD of $FeCl_3$ with subsequent washing and calcination. An iron excess (Fe/Al >1) does not necessarily lead to more extensive clustering (cf. Fe–Z(B)). EXAFS and Mössbauer spectroscopy agree in detecting the presence of γ-Fe_2O_3 structures in the larger aggregates.

On the other hand, Mössbauer spectroscopy and TPR indicate a much larger extent of clustering than do EXAFS and XRD, although the aggregate size found by Mössbauer spectroscopy is even larger than that inferred from the TPR data (hydrogen consumption ratio between high- and low-temperature peaks). Moreover, the extent of aggregation suggested by the TPR traces shows variations that are not reflected either by EXAFS or by Mössbauer spectroscopy, in particular with Fe–Z(A, W_{10}, $C_{0.5}$), the TPR result of which indicates the predominance of well-dispersed iron. The latter was so surprising that the very sample studied by Mössbauer spectroscopy was subsequently also subjected to TPR (trace f′ in Fig. 7) to prove the sample identity. Although the accuracy of this run was low due to violation of the Monti–Baiker criterion (small sample amount), it is quite clear that the TPR trace indicating a very small extent of clustering was reproduced.

The most significant contradictions occur between the results of EXAFS and Mössbauer spectroscopy. In EXAFS, the scattering contribution of higher shells, which can be nicely observed in the pure oxides and also in Fe–Z(A, SSIE, nW), are near the detection limit or hardly significant at all in the remaining samples (cf. Fig. 5). Mössbauer spectroscopy, however, detects ≈50% of the iron (still 35% in Fe–Z(B)) in large particles whereas EXAFS sees almost no order beyond $R = 0.4$ nm. Both conclusions are supported by the results of a second technique. Aggregates exhibiting magnetic splitting at 78 K are several nanometers in size and should therefore be detectable by XRD, but no Fe_2O_3 reflectances were found in representative samples (cf. Fig. 3). On the other hand, the high H/Fe ratios obtained by TPR, though with limited accuracy, indicate a high clustering degree except for Fe–Z(A, W_{10}, $C_{0.5}$). This result was expected in view of the high intensity of the Brønsted signal found by IR (Fig. 2), which indicates a significant extent of aggregation. In TPR, the difference between experimental H/Fe values and H/Fe = 3 should account only for those Fe^{3+} ions that are attached to cation sites. The high reduction degree found with Fe–Z(B), where Mössbauer spectroscopy detected fewer clusters, may arise from the participation of the silanol defect sites in anchoring the iron species, as was recently reported for Fe–MCM-41 materials (35). This might have led to a smaller size of the majority of clusters, and upon reduction those Fe ions attached to silanol groups are probably completely reduced during TPR.

There are two effects that may explain the contradictions between the results of TPR, EXAFS, and Mössbauer spectroscopy. EXAFS (and XRD) may fail to see the aggregates due to their high defectivity. XPS and XRD (attenuation of reflectances at $2\Theta = 8.9$ and 8.0°) suggest that the iron phase is largely intrazeolite in all catalysts. This includes the

clustered species indicated by TPR, which may extend in size to those found by Mössbauer spectroscopy. The growth of such aggregates is interfered by the zeolite framework, which is destroyed during aggregation and may render inclusions and other defects. Such disorder will disturb coherence in XRD and smear out scattering signals in EXAFS. On the other hand, it will not prevent magnetic coupling, but it may contribute to Mössbauer parameters deviating from those of the reference phases, which has complicated the assignment of several signals (30, 31).

On the other hand, it has been mentioned above that the fraction of recoil-free absorption (reflected by the Debye temperature) should differ significantly between single Fe ions or oligomers and large oxide aggregates, which leads to an overestimation of the aggregate contribution. The fact that Mössbauer spectroscopy finds an aggregation degree of >50% in a material (Fe–Z(A, W_{10}, $C_{0.5}$)) for which TPR shows a very small clustering tendency both by the reduction degree H/Fe and by the profile shape suggests that the distortion in the distribution of species caused by the different Debye temperatures is serious: In Fe–Z(A, W_{10}, $C_{0.5}$) the aggregated phases probably cover only 10–20% of the iron present. It appears, therefore, that with overexchanged Fe–ZSM-5 materials Mössbauer spectroscopy is focused on the large aggregates while EXAFS is most sensitive to the disperse structures. This implies that Mössbauer spectroscopy predominantly looks at species that are not likely to be the active sites searched for (*vide infra*). On the other hand, it will sensitively indicate uncontrolled clustering processes: the same catalysts did not exhibit any sextet signal after the CVD step, i.e., before washing and calcination (32).

Hence, the discussion of the Fe species present has to rely mainly on the TPR results, although the remaining techniques provide valuable supplementary information. From their large H/Fe value in TPR and their TPR profiles, Fe–Z(A), Fe–Z(A, C_{10}), Fe–Z(A, $C_{0.5}$), and Fe–Z(B) appear to contain considerable amounts of disperse but clustered phases, probably ill structured, but also large aggregates, as detected by Mössbauer spectroscopy. On the other hand, the Fe–Fe coordination numbers <1 found with these materials by EXAFS imply that there is also a significant amount of isolated Fe ions. It may appear from the TPR results that Fe–Z(A, W_{10}, $C_{0.5}$) contains almost exclusively monomeric iron ions, but the still-large intensity of the Brønsted signal in the IR spectrum (Fig. 2) indicates the presence of a significant amount of clustered species also in this case. This contradiction may be resolved by assuming (as has been implicitly done by previous authors) that in Fe–O–Fe dimers the second Fe ion, which is originally detached from its cation site, giving rise to the appearance of a Brønsted proton, returns to its original site upon reduction to Fe^{2+} and thus escapes further reduction to Fe(0). The rather high Fe–Fe coordination numbers derived for this sample might indicate the presence of a particular order of this type, but by analogy with the other materials, the existence of monomeric ions has to be assumed also in this sample with the lowest clustering degree of the Fe species. Indeed, the presence of a significant fraction (20%) of isolated Fe sites in Fe–ZSM-5 prepared by CVD of $FeCl_3$ was recently demonstrated with magnetization measurements for a material in which EXAFS analysis gave a Fe–Fe coordination number of 1 (23), and a complicated site structure of a catalyst with a TPR profile similar to that of Fe–Z(A, W_{10}, $C_{0.5}$) (6) is invoked by ESR spectra shown in (10).

In summary, the Fe–ZSM-5 catalysts prepared by CVD of $FeCl_3$ into H–ZSM-5(A) obviously contain iron in a multitude of species of different aggregation degree, from isolated ions via dimers, oligomers, and clusters, to large aggregates. The aggregation is most likely facilitated by residual chlorine, as was anticipated in (23). Probably, those species that still carry Cl ligands after washing become mobile at higher temperatures. There is a dependence of the cluster structure on the calcination conditions, which seems, however, to be of little relevance to the catalytic behavior (*vide infra*). The clustering tendency is largely suppressed by extensive washing prior to calcination.

Fe/Al ratios >1 were achieved by SSIE and by CVD of $FeCl_3$ into a zeolite with a large number of silanol groups (Fe–Z(B)). It was mentioned above that in the latter case the silanol groups (in particular those in silanol nests) apparently provided additional anchors for the iron species. Although the IR band of interacting silanol groups at 3730 cm^{-1} was not recovered after calcination (and catalysis (18)), no isolated Fe^{3+} in tetrahedral coordination was found by Mössbauer spectroscopy. This may indicate that the iron in these sites served as additional nuclei for aggregation, thus being incorporated into clusters. In the case of Fe–Z(A, SSIE, *n*W), strong aggregation was observed even by EXAFS. Unfortunately, no Mössbauer spectrum is available for this material, but in a catalyst resulting from a faulty batch prepared according to the standard procedure, ≈80% of the iron was found in magnetically coupled aggregates by Mössbauer spectroscopy while the EXAFS spectrum was similar to that of Fe–Z(A, SSIE, *n*W). Remarkably, this faulty preparation still yielded a peak NO conversion of 60% (31).

The Fe species in Fe–Z(Aq) can be described as well dispersed, with some clustering, which is again detected by TPR, but not by EXAFS (18). A large amount of Brønsted acidity is available despite the considerable Fe content (2.4 wt%), which indicates that the Fe ions carry extralattice oxygen.

Regarding the catalytic properties, it should be noted that a significant basic activity is achieved simply by mixing Fe_2O_3 with H–ZSM-5 (Fig. 1B). The discussion will mainly concern the extra activity giving rise to higher NO conversions, between 673 and 523 K, which was found with all

catalysts prepared by interaction of $FeCl_3$ with H–ZSM-5(A). The most prominent result is that the catalytic performance is not significantly changed when a considerable part of the Fe species is aggregated. Even Fe–Z(A, SSIE, *n*W), which was used without any washing step and showed heavy aggregation of the iron phase, still achieved a peak NO conversion of ≈60%. This shows that the aggregates are not the active sites since the catalytic performance is not deteriorated when their amount is decreased. On the other hand, in Fe–ZSM-5 with well-dispersed Fe species, a significant part of the iron does not contribute to the extra activity since there is no adverse effect of partial clustering. Thus, the extra activity in the 673- to 523-K temperature range has to be ascribed to a minority site containing iron in highly dispersed form.

While the data reported in the present study do not permit making suggestions about the nature of this site, we refer to recent research by our group, where it was found that highly active, probably isolated Fe sites may be formed by mechanochemical treatment of a $FeCl_3$/H–ZSM-5 mixture. With these catalysts, reaction rates comparable to those reported in the present study with an order of magnitude less iron (11). High activites with Fe—ZSM5 of low Fe content were also reported in (36) for SCR with propane. We suppose that these sites contribute most of the catalytic activity: a strong dependence of SCR activity on the specific site occupied by a cation was recently demonstrated for Co ions by Kaucky *et al*. (37). In overexchanged Fe–ZSM-5, other iron species, e.g., different monomer sites, dimers, and oligomers, may add to the SCR activity and cause a certain downward shift of the conversion-temperature curve between Fe–ZSM-5 of low and high Fe content, which was described in (11). Monomeric Fe^{3+} sites would probably bear an extralattice oxygen atom (FeO^+). They should be easily reduced in hydrogen ($\rightarrow FeOH^+$), while interaction with CO would render the unstable Fe^+ ion (6). Little is known about their interaction with hydrocarbons, which is probably one of their functions in the reaction cycle.

Finally, the data presented above permit some conclusions concerning the role of the Brønsted sites in the SCR of NO with isobutane over Fe–ZSM-5. As to the catalytic behavior of the Fe_2O_3/H–ZSM-5 mixture, this catalyst completely lost its ability to activate isobutane when the protons were poisoned by alkali ions introduced by solid-state ion exchange (27). Thus, the physical mixture most likely reduces NO in a process in which isobutane is activated over zeolite protons and then attacked by NO_2 formed over Fe sites. The process that gives rise to the extra activity between 673 and 523 K (Fig. 1B) may be different; i.e., it may proceed over *particular* Fe sites (*vide supra*) with or without cooperation by Brønsted sites. It may, however, also be analogous to the mechanism providing the basic activity, being strongly favored by the close proximity of (unspecific) iron sites and protons; i.e., the higher conversions would then arise from the minimization of the diffusion path for NO_2 in the reaction mechanism observed with the physical mixture. The latter assumption can be falsified by the results obtained with Fe–Z(Aq) (11): this material exhibits a low activity, although the iron is well dispersed and most of the Brønsted acidity is available.

The question of whether the Fe sites responsible for the peak SCR activity require the cooperation of acidic protons is not easy to address. Acidity poisoning strategies run the risk of affecting the Fe sites as well. The results obtained with Fe–Z(B) may shed some light on the problem. The low basic NO conversion achieved with this catalyst between 823 and 673 K (cf. Fig. 1B) is, certainly, a consequence of its low acidity. But also, below 673 K, where extra activity is seen with most Fe–ZSM-5 catalysts, there is no noticeable increase with Fe–Z(B). This may be due to the shortage of Brønsted sites as well, or the iron sites required may not have been formed in this matrix. The remarkable capability of Fe–Z(B) for isobutane activation (isobutane conversion exceeding that of the Fe_2O_3/H–ZSM-5 mixture (Fig. 1B)) may indicate that it is rather the shortage of Brønsted sites that impedes the SCR reaction, i.e., that the SCR of NO by isobutane is a bifunctional reaction over the whole temperature range studied. The Brønsted sites could be required to catalyze the hydrolysis of nitrile intermediates to produce ammonia, which is probably the reaction partner in the N–N coupling step required to produce N_2, according to recent mechanistic studies of Chen *et al.* (38).

CONCLUSIONS

Overexchanged Fe–ZSM-5 catalysts were prepared by interaction of $FeCl_3$ with H–ZSM-5 under differing conditions (chemical vapor deposition, with variation in washing and calcination conditions, or solid-state ion exchange) and into parent zeolites of differing properties (abundance of lattice defects). Their structural properties were investigated by spectroscopic techniques (EXAFS, Mössbauer spectroscopy, IR XPS), XRD, and TPR and correlated with their catalytic behavior in the SCR of NO by isobutane. It was found that the characterization of such catalysts requires the combination of several techniques, since the exclusive use of one method (e.g., EXAFS or Mössbauer spectroscopy) would have resulted in erroneous conclusions.

Extensive washing prior to the final calcination step is essential to producing highly dispersed intrazeolite Fe species, although the formation of larger aggregates upon calcination is hard to avoid at the Fe contents used. Less-extensive washing results in a more intense clustering tendency resulting in (intrazeolite) Fe oxide clusters of wide size distribution and ill-defined long-range order. The clustering is probably favored by residual chlorine rendering Fe species mobile. Fe–ZSM-5 with Fe/Al >1 can be easily prepared

by solid-state ion exchange or by CVD into ZSM-5 with a large amount of lattice defects, e.g., silanol nests.

The catalytic behavior of Fe–ZSM-5 systems in the SCR of NO with isobutane should be differentiated into a basic activity, which is obtained merely by mixing Fe_2O_3 with H–ZSM-5, and an extra activity between 673 and 523 K, which may arise from particular sites. The former is completely poisoned by alkali ions. Our results show that the origin of the latter in overexchanged Fe–ZSM-5 prepared by interaction of $FeCl_3$ with H–ZSM-5 is not simply a better distribution of Fe species over the zeolite crystal to minimize diffusion paths of intermediates (NO_2), but the presence of a particular site. This site is a minority species of the iron phase, since there was no dramatic effect on the catalytic behavior when a significant part of the iron phase was present in aggregates. On the basis of recent reports in the literature (11, 38) it is suggested that this site is an isolated Fe species. The remaining Fe species merely modify the catalytic properties.

A Fe–ZSM-5 catalyst prepared with a defective Fe–ZSM-5 matrix, in which the dispersion of the Fe phase was comparable to that in most other materials prepared, was inferior even to the Fe_2O_3/H–ZSM-5 mechanical mixture in NO conversion but exceeded it in isobutane activation. This may indicate that not only the basic activity but also the extra activity requires the cooperation of redox and acidic sites.

ACKNOWLEDGMENTS

We are grateful for experimental contributions by Mrs. S. Wiedemeyer (TPR), Mrs. A. Gomann (IR), and Mr. M. Schwidder and for consultation by Prof. D.C. Koningsberger, Dr. T. Ressler, and Dr. K.V. Klementiev, in particular regarding problems of EXAFS analysis. Financial support for C.S. by the Deutsche Forschungsgemeinschaft (Graduiertenkolleg "Dynamic Processes at Solid Surfaces") is gratefully acknowledged.

REFERENCES

1. Fritz, A., and Pitchon, V., *Appl. Catal. B* **13**, 1 (1997).
2. Parvulescu, V. I., Grange, P., and Delmon, B., *Catal. Today* **46**, 233 (1998).
3. Traa, Y., Burger, B., and Weitkamp, J., *Microporous Mesoporous Mater.* **30**, 3 (1999).
4. Feng, X., and Hall, W. K., *Catal. Lett.* **41**, 45 (1996).
5. Hall, W. K., Feng, X., Dumesic, J., and Watwe, R., *Catal. Lett.* **52**, 13 (1998).
6. Chen, H.-Y., and Sachtler, W. M. H., *Catal. Today* **42**, 73 (1998).
7. Marturano, P., Drozdova, L., Kogelbauer, A., and Prins, R., *J. Catal.* **192**, 236 (2000).
8. Battiston, A. A., Bitter, J. H., and Koningsberger, D. C., *Catal. Lett.* **66**, 75 (2000).
9. Joyner, R. W., and Stockenhuber, M., *J. Phys. Chem. B* **103**, 5963 (1999).
10. Chen, H.-Y., El-Malki, E.-M., Wang, X., Van Santen, R. A., and Sachtler, W. M. H., *J. Mol. Catal. A* **162**, 159 (2000).
11. Heinrich, F., Schmidt, C., Löffler, E., and Grünert, W., *Catal. Commun.* **2**, 317 (2001).
12. Wagner, C. D., *in* "Practical Surface Analysis" (D. Briggs and M. P. Seah, Eds.), Vol. 1, p. 635. Wiley, Chichester, U.K., 1990.
13. Ressler, T., *J. Phys. IV France* **7**, C2-269 (1997).
14. Zabinsky, S. I., Rehr, J. J., Ankudinov, A., Albers, J. C., and Eller, M. J., *Phys. Rev. B* **52**, 2995 (1995).
15. Monti, D. A. M., and Baiker, A., *J. Catal.* **83**, 323 (1983).
16. Löffler, E., Lohse, U., Peuker, C., Oehlmann, G., Kustov, L. M., Zholobenko, V. L., and Kazansky, V. B., *Zeolites* **10**, 266 (1990).
17. Chen, H.-Y., Voskoboinikov, T., and Sachtler, W. M. H., *Catal. Today* **54**, 483 (1999).
18. Heinrich, F., Löffler, E., and Grünert, W., *Stud. Surf. Sci. Catal.* **135**, 30-P-15 (2001).
19. Heinrich, F., Schmidt, C., Löffler, E., and Grünert, W., unpublished results.
20. Calas, G., and Petiau, J., *Solid State Commun*. **48**, 625 (1983).
21. Schmidt, C., Ph.D. thesis. Ruhr-Universität Bochum, 2001.
22. Inorganic Crystal Structure Database, FIZ Karlsruhe/NIST.
23. Marturano, P., Drozdova, L., Pirngruber, D., Kogelbauer, A., and Prins, R., *Phys. Chem. Chem. Phys.* **3**, 5585 (2001).
24. Okamoto, Y., Kikuta, H., Ohto, Y., Nasu, S., and Terasaki, O., *Stud. Surf. Sci. Catal.* **105**, 2051 (1997).
25. Lee, H.-T., and Rhee, H.-K., *Catal. Lett.* **61**, 71 (1997).
26. Wimmers, O. J., Arnoldy, P., and Moulijn, P. A., *J. Phys. Chem.* **90**, 1331 (1986).
27. Heinrich, F., Wischnewski, S., Löffler, E., and Grünert, W., unpublished results.
28. Joyner, R. W., and Stockenhuber, M., *Catal. Lett.* **45**, 15 (1998).
29. Inamura, K., Iwamoto, R., Iino, A., and Takyu, T., *J. Catal.* **142**, 273 (1993).
30. Menzel, M., Heinrich, F., Schmidt, C., Löffler, E., Grünert, W., and Mehner, W., presented at Fifth Seeheim Workshop on Mössbauer Spectroscopy, Seeheim/Germany May 21–25, 2002.
31. Heinrich, F., Ph.D. thesis. Ruhr-Universität Bochum, 2002.
32. Menzel, M., Heinrich, F., and Grünert, W., unpublished results.
33. Bauminger, R. E., Levy, A., Labenski de Kaner, F., Ofer, S., and Heitner-Wirguin, C., *J. Phys.* **41**, C1-329 (1980).
34. Lazar, K., Kotasthane, A. N., and Fejes, P., *Catal. Lett.* **57**, 171 (1999).
35. Stockenhuber, M., Hudson, M. J., and Joyner, R. W., *J. Phys. Chem. B* **194**, 3370 (2000).
36. Sobalik, Z., Vondrova, A., Tvaruskova, Z., and Wichterlova, B., *Catal. Today* **75**, 347 (2002).
37. Kaucky, D., Vondrova, A., Dedecek, J., and Wichterlova, B., *J. Catal.* **194**, 318 (2000).
38. Chen, H.-Y., Voskoboinikov, T., and Sachtler, W. M. H., *J. Catal.* **186**, 91 (1999).